

# Retention Time Prediction Using Neural Networks Increases Identifications in Crosslinking Mass Spectrometry

Sven H. Giese<sup>\*1,3,4</sup>, Ludwig R. Sinn<sup>\*1</sup>, Fritz Wegner<sup>1</sup>, and Juri Rappsilber<sup>†1,2</sup>

<sup>1</sup> Bioanalytics, Institute of Biotechnology, Technische Universität Berlin, 13355 Berlin, Germany

<sup>2</sup> Wellcome Centre for Cell Biology, School of Biological Sciences, University of Edinburgh, Edinburgh EH9 3BF, United Kingdom

<sup>3</sup> Data Analytics and Computational Statistics, Hasso Plattner Institute for Digital Engineering

<sup>4</sup> Digital Engineering Faculty, University of Potsdam

## Abstract

Crosslinking mass spectrometry (Crosslinking MS) has developed into a robust technique that is increasingly used to investigate the interactomes of organelles and cells. However, the incomplete and noisy information in the spectra limits the numbers of protein-protein interactions (PPIs) that can be confidently identified. Here, we successfully leveraged chromatographic retention time (RT) information to aid the identification of crosslinked peptides from spectra. Our Siamese machine learning model xiRT achieved highly accurate RT predictions of crosslinked peptides in a multi-dimensional separation of crosslinked *E. coli* lysate. We combined strong cation exchange (SCX), hydrophilic strong anion exchange (hSAX) and reversed-phase (RP) chromatography and reached  $R^2$  0.94 in RP and a margin of error of 1 fraction for hSAX in 94%, and SCX in 85% of the predictions. Importantly, supplementing the search engine score with retention time features led to a 1.4-fold increase in PPIs at a 1% false discovery rate. We also demonstrate the value of this approach for the more routine analysis of a crosslinked multiprotein complexes. An increase of 1.7-fold in heteromeric crosslinked residue-pairs was achieved at 1% residue-pair FDR for Fanconi anaemia monoubiquitin ligase complex, solely using reversed-phase RT. Retention times are a powerful complement to mass spectrometric information to increase the sensitivity of Crosslinking MS analyses.

---

\* authors contributed equally

† corresponding author: [juri.rappsilber@tu-berlin.de](mailto:juri.rappsilber@tu-berlin.de)

## 25 Introduction

26 Crosslinking mass spectrometry (Crosslinking MS) reveals the topology of proteins, protein complexes,  
27 and protein-protein interactions.<sup>1</sup> Fueled by experimental and computational improvements, the field  
28 is moving towards the analyses of interactomes of organelles and cells.<sup>1-3</sup> The identification of  
29 crosslinked peptides poses three major challenges. First, the low abundance of crosslinked peptides  
30 compared to linear peptides decreases their chance for mass spectrometric observation. Second, the  
31 unequal fragmentation of the two peptides leads to a biased total crosslinked peptide spectrum match  
32 (CSM) score<sup>4,5</sup>. Third, the combinatorial complexity from searching all the possible peptide pairs in a  
33 sample increases the chance for random matches. These challenges increase from the analysis of  
34 individual proteins to organelles and cells.

35 To address the challenge of low abundance, Crosslinking MS studies routinely rely on chromatographic  
36 methods to enrich and fractionate crosslinked peptides<sup>1,2,6</sup>. Essentially all analyses contain at least one  
37 chromatographic step, by directly coupling reversed-phase (RP) chromatography separation to the  
38 mass spectrometer (LC-MS). Additional separation is frequently employed when more complex  
39 systems are being analysed. Strong cation exchange chromatography (SCX)<sup>7,8</sup> was used for the analysis  
40 of HeLa cell lysate<sup>9</sup> or murine mitochondria<sup>10</sup>. Size-exclusion chromatography (SEC)<sup>11</sup> was used to  
41 fractionate crosslinked HeLa cell lysate<sup>12</sup> and *Drosophila melanogaster* embryos extracts<sup>13</sup>. Multi-  
42 dimensional peptide pre-fractionation was used for the analysis of crosslinked human mitochondria  
43 (SCX-SEC)<sup>14</sup> and *M. pneumoniae* (SCX-hSAX)<sup>15</sup>. Such multi-dimensional chromatography workflows can  
44 yield in the order of 10,000 CSM at 1-5% false discovery rate (FDR).<sup>14-17</sup>

45 The identification of crosslinked peptides from spectra is however still challenged by the uneven  
46 fragmentation of the two peptides and the large search space that increase the odds of random  
47 matches. This is especially the case for heteromeric crosslinks as the size of their search space exceeds  
48 that of self-links, i.e. links falling within a protein or homomer<sup>16</sup>. Typically, database search tools use  
49 the precursor mass and fragmentation spectrum for the identification of peptides to compute a single

50 final score for each CSM. For linear peptides, post-search methods such as Percolator<sup>18</sup> have been  
51 developed that train a machine learning predictor to discriminate correct from incorrect peptide  
52 identification. Percolator uses additional spectral information (features) such as charge, length, and  
53 other enzymatic descriptors of the peptide<sup>19</sup> to compute a final support vector machine (SVM) score.  
54 Similarly, the crosslink search engine Kojak<sup>20</sup> supports the use of PeptideProphet<sup>21,22</sup> and XlinkX<sup>23</sup>  
55 supports Percolator<sup>18</sup>, while pLink2<sup>24</sup> and ProteinProspector<sup>4</sup> have a built-in SVM classifier to re-rank  
56 CSMs. Although RT data is readily available, none of these tools use the, often multi-dimensional, RT  
57 information for improved identification in crosslinking studies. A prerequisite for this would be that  
58 retention times could be predicted reliably.

59 For linear peptides, RT prediction has been implemented under various chromatographic conditions.<sup>25–</sup>  
60 <sup>31</sup> In contrast, RTs of crosslinked peptides have not been predicted yet. A suitable machine learning  
61 approach for this could be deep learning<sup>32</sup>. Deep neural networks have been successfully applied in  
62 proteomics, for example for de novo sequencing<sup>33</sup> or for the prediction of retention times<sup>29,34</sup> and  
63 fragment ion intensities<sup>35</sup>. Deep learning allows encoding peptide sequences very elegantly through,  
64 for example, recurrent neural network (RNN) layers. These layers are especially suited for sequential  
65 data and are common in natural language processing<sup>32</sup>. RNNs use the order of amino acids in a peptide  
66 to generate predictions without additional feature engineering. However, it is unclear how to encode  
67 the two peptides of a crosslink.

68 Moreover, it is also unclear whether the knowledge of RTs could improve the identification of  
69 crosslinked peptides. A common scenario for an identified crosslink is that one of its peptides was  
70 matched with high sequence coverage, while the other was matched with poorer sequence coverage.<sup>4</sup>  
71 Such CSMs unfortunately resemble matches where one peptide is correct and the other is false (i.e. a  
72 target-decoy match or a true target and false target match). Another consequence of coverage gaps is  
73 the misidentification of noncovalently associated peptides as crosslinks.<sup>36</sup> The severity of this coverage  
74 issue depends on the applied acquisition strategy<sup>37</sup>, crosslinker chemistry<sup>38</sup>, and the details of the  
75 implemented scoring in the search engine. Nevertheless, assuming RT predominantly depends on both

76 peptides of a crosslink, it could complement mass spectrometric information and thus improve existing  
77 scoring routines and lead to more crosslinks at the same confidence (i.e. constant FDR).

78 In this study, we prove that analytical separation behavior carries valuable information about both  
79 crosslinked peptides and can improve the identification of crosslinks. For this we built a multi-  
80 dimensional RT predictor for crosslinked peptides based on a proteome-wide crosslinking experiment  
81 comprising 144 acquisitions on an Orbitrap mass spectrometer from extensively fractionated peptides  
82 of the soluble high-molecular weight proteome of *E. coli*. We then investigated the benefits of  
83 incorporating the derived RT predictions into the identification process. In addition, we demonstrate  
84 the value of RT prediction for a purified multiprotein complex using the reversed-phase  
85 chromatography dimension only.

## 86 Material and Methods

### 87 Sample Preparation

88 Crosslink samples were processed exactly as described in Lenz *et al.*<sup>16</sup> with the exception that the  
89 crosslinker DSS was used. Briefly, cells were lysed by sonication, cleared from debris and the high-  
90 molecular weight proteome enriched by ultrafiltration. This sample was then fractionated by size-  
91 exclusion chromatography to give 44 fractions. The proteins of each fraction were crosslinked at 0.75  
92 mM DSS. The crosslinked samples were pooled and precipitated using acetone. Upon resuspending,  
93 the samples were derivatized by incubating 30 minutes at room temperature with 10 mM  
94 dithiothreitol followed by 20 mM iodoacetamide and proteolyzed using LysC and Trypsin. The digests  
95 were fractionated, first, by strong cation exchange chromatography (9 fractions) and the obtained  
96 fractions separated by hydrophilic strong anion exchange chromatography as the second separation  
97 dimension (10 pools). Samples were cleaned up in between and at the end of the procedures  
98 following the StageTip protocol<sup>39</sup>.



## 99 Spectra & Peptide Spectrum Match Processing

100 All raw spectra were converted to Mascot generic format (MGF) using msConvert<sup>40</sup>. The database  
101 search with Comet<sup>41</sup> (v. 2019010) was done with the following settings: peptide mass tolerance 3  
102 ppm; isotope\_error 3; fragment bin 0.02; fragment offset 0.0; decoy\_search 1; fixed modification on  
103 C (carbamidomethylation, +57.021 Da); variable modifications on M (oxidation, +15.99 Da). False  
104 discovery rate (FDR) estimation was performed for each acquisition. First, the highest scoring PSM  
105 for a modified peptide sequence was selected, then the FDR was computed based on Comet's e-  
106 value. Spectra were searched using xiSEARCH (v. 1.6.753)<sup>12</sup>, after recalibration of precursor and  
107 fragment m/z values, with the following settings: precursor tolerance, 3 ppm; fragment tolerance, 5  
108 ppm; missed cleavages, 2; missed monoisotopic peaks<sup>42</sup>, 2; minimum peptide length, 7; variable  
109 modifications: oxidation on M, mono-links for linear peptides on K,S,T,Y, fixed modifications:  
110 carbamidomethylated C. The specificity of the crosslinker DSS was configured to link K, S, T, Y, and  
111 the protein N-terminus with a mass of 138.06807 Da. The searches were run with the workflow  
112 system snakemake<sup>43</sup>. The FDR on CSM-level was defined as  $FDR = TD - DD / TT$ <sup>44</sup>, where TD indicates  
113 the number of target-decoy matches, DD the number of decoy-decoy matches and TT the number of  
114 target-target matches. Crosslinked peptide spectrum matches (CSMs) with non-consecutive peptide  
115 sequences were kept for processing<sup>45</sup>. PPI level FDR computation was done using xiFDR<sup>44</sup> (v. 2.1.3  
116 and 2.1.5 for writing mzIdentML) to an estimated PPI-FDR of 1%, disabling the boosting and filtering  
117 options. CSM, peptide and residue-level FDR were fixed at 5%, protein group FDR was set to 100%.  
118 FDR estimations for self and heteromeric links were done separately. In xiFDR a unique CSM is  
119 defined as a combination of the two peptide sequences including modifications, link sites and  
120 precursor charge state. For the assessment of identified CSMs an entrapment database (described in  
121 the next section) as well as decoy identifications were used on both, CSM and PPI levels. PPI results  
122 were also compared against the APID<sup>46</sup> and STRING<sup>47</sup> databases (v11, minimal combined confidence  
123 of 0.15).

## 124 Database Creation

125 The database of potentially true crosslinks was defined as *Escherichia coli* proteome (reviewed  
126 entries from Uniprot release 2019-08). This database was filtered further to proteins identified with  
127 at least a single linear peptide at a q-value<sup>48</sup> threshold of 0.01,  $q(t) = \min_{s \leq t} FDR(s)$ , with the  
128 threshold  $t$  and score  $s$ . This resulted in 2850 proteins. In addition to the FDR estimation through a  
129 decoy database, we used an entrapment database. The proteins from the entrapment database  
130 represent the search space of false positive CSMs independent of *E. coli* decoys and were sampled  
131 from human proteins (UP000005640, retrieved 2019-05). *E. coli* decoys might fail in this task after  
132 machine learning if overfitting should have taken place. So, entrapment targets allow control for  
133 overfitting. For this, human target peptides were treated as targets and human decoy peptides as  
134 decoys. To avoid complications through false spectrum matches due to homology, we used blastp<sup>49</sup>  
135 (BLAST 2.9.0+, blastp-short mode, word size 2, e-value cutoff 100) and aligned all *E. coli* tryptic  
136 peptides (1 missed cleavage, maximum length 100) to the human reference. All proteins that showed  
137 peptide alignments with a sequence identity of 100% were removed from the human database. Only  
138 the remaining 9990 sequences were used as candidates in the entrapment database. For each of the  
139 2850 *E. coli* proteins a human protein was added to the database. To reduce search space biases  
140 from protein length and thus different number of peptides for the two organisms, we followed a  
141 special sampling strategy. The human proteins were selected by a greedy nearest neighbor approach  
142 based on the K/R counts and the sequence length. The final number of proteins in the combined  
143 database (*E. coli* & human) was 5700 (2850\*2).

## 144 Fanconi anaemia monoubiquitin ligase complex data processing

145 The publicly available raw files from an analysis of the BS3-crosslinked Fanconi anemia  
146 monoubiquitin ligase complex<sup>50</sup> (FA-Complex) were downloaded from PRIDE together with the  
147 original FASTA file (PXD014282). The raw files were processed as described for the *E. coli* data (m/z  
148 recalibration and searched with xiSEARCH), followed by an initial 80% CSM-FDR filter for further  
149 processing. Due to the much smaller FASTA database (8 proteins), the entrapment database was  
150 constructed more conservative than for the proteome-wide *E. coli* experiment, i.e. for each of the  
151 target proteins, the amino acid composition was used to retrieve the nearest neighbor in an *E. coli*  
152 database. The FDR settings to evaluate the rescoring were set to 5% CSM- and peptide-pair level FDR,  
153 1% residue-pair- and 100% PPI-FDR using xiFDR without boosting or additional filters. The resulting  
154 links were visualized (circular view) and mapped to an available 3D structure (final refinement model  
155 'sm.pdb')<sup>51,52</sup> using xiVIEW<sup>53</sup>. To ease the comparison of identified and random distances, a random  
156 Euclidean distance distribution was derived in three steps: first, all possible crosslinkable residue-pair  
157 distances in the 3D structure were computed. Second, 300 random 'bootstrap' samples with n  
158 distances were drawn (n= the number of identified residue-pairs at a given FDR) and third, the mean  
159 per distance bin was computed across all 300 samples.

## 160 xiRT - 3D Retention Time Prediction

161 The machine learning workflow was implemented in python and is freely available from  
162 <https://github.com/Rappsilber-Laboratory/xiRT>. xiRT is the successor of DePART<sup>29</sup>, which was  
163 developed for the retention time (RT) prediction of hSAX fractionated peptides based on pre-  
164 computed features. xiRT makes use of modern neural network architectures and does not require  
165 feature engineering. We used the popular python packages sklearn<sup>54</sup> and TensorFlow<sup>55</sup> for processing  
166 (section S1 for more details). xiRT consists of five components (Fig. 1d, Fig. S1, Section S1): (1) The  
167 input for xiRT are amino acid sequences with arbitrary modifications in text format (e.g. Mox for  
168 oxidized Methionine). xiRT uses a similar architecture for linear and crosslinked peptide RT  
169 prediction. Before the sequences can be used as input for the network, the sequences are label

170 encoded by replacing every amino acid by an integer and further 0-padded to guarantee that all  
171 input sequences have the same length. Modified amino acids as well as crosslinked residues are  
172 encoded differently than their unmodified counterparts. (2) The padded sequences were then  
173 forwarded into an embedding layer that was trained to find a continuous vector representation for  
174 the input. (3) To account for the sequential structure of the input sequences, a recurrent layer was  
175 used (either GRU or LSTM). Optionally, the GRU/LSTM layers were followed by batch normalization  
176 layers. For crosslinked peptide input, the respective outputs from the recurrent layers were then  
177 combined through an additive layer (default setting). (4) Task-wise subnetworks were added for  
178 hSAX, SCX, and RP retention time prediction. All three subnetworks had the same architecture: three  
179 fully connected layers, with dropout and batch normalization layers between them. The shape of the  
180 subnetworks is pyramid-like, i.e. the size of the layers decreased with network depth. (5) Each  
181 subnetwork had its own activation function. For the RP prediction, a linear activation function was  
182 used and mean squared error (*MSE*) as loss function. For the prediction of SCX and hSAX fractions we  
183 followed a different approach. The fraction variables were encoded for ordinal regression in neural  
184 networks<sup>56</sup>. For example, in a three-fraction setup, the fractions (*f*) were encoded as  $f_1 =$   
185  $[0, 0, 0]$ ,  $f_2 = [1, 0, 0]$  and  $f_3 = [1, 1, 0]$ . Subsequently, we chose sigmoid activation functions for the  
186 prediction layers and defined binary cross entropy (*BC*) as loss function. To convert predictions from  
187 the neural network back to fractions, the index of the first entry with a predicted probability of less  
188 than 0.5 was chosen as the predicted fraction. The overall loss was computed by a weighted sum of  
189 the  $MSE_{RP}$ ,  $BC_{SCX}$  and  $BC_{hSAX}$ . The weight parameters are only necessary when xiRT is used to  
190 predict multiple RT dimensions at the same time (multi-task). To predict a single dimension (single-  
191 task, e.g. RP only), the weight can be set to 1. The number of neurons, dropout rate, intermediate  
192 activation functions, the weights for the combined loss, number of epochs and other parameters in  
193 xiRT were optimized on linear peptide identification data. Reasonable default values are provided  
194 within the xiRT package. For optimal performance, further optimization might be necessary for a  
195 given task.

## 196 Cross-Validation and Prediction Strategy

197 Cross-validation (CV) is a technique to estimate the generalization ability of a machine learning  
198 predictor<sup>57</sup> and is often used for hyper-parameter optimization. We performed a 3-fold CV for the  
199 hyper-parameter optimization on the linear peptide identification data from xiSEARCH, excluding all  
200 identifications to the entrapment database (section S2 and Fig. S2 for details). We defined a coarse  
201 grid of parameters (Tab. S1) and chose the best performing parameters based on the average total  
202 (unweighted) loss,  $R_{RP}^2$  and accuracy across the CV folds. Further, we define the relaxed accuracy  
203 (racc) to measure how many predictions show a lower prediction error than  $|1|$ . We then repeated  
204 the process with an adapted set of parameters (Tab. S2). In addition to the standard CV strategy, we  
205 used a small adjustment: per default, in k-fold cross-validation, the training split consists of k-1 parts  
206 of the data (folds) and a single testing fold. However, we additionally used a fraction (10%) from the  
207 training folds as extra validation set during training. The validation set was used to select the best  
208 performing classifier over all epochs. The model assessment was strictly limited to the testing folds.  
209 This separation into training, validation and testing was also used for the semi-supervised learning  
210 and prediction of RTs, i.e. when xiRT was used to generate features to rescore CSMs previously  
211 identified from mass spectrometric information. In this scenario, the CV strategy was employed to  
212 avoid the training and prediction on the same set of CSMs. In xiRT, a unique CSM is defined as  
213 combination of the two peptide sequences, ignoring link sites and precursor charge.

## 214 Supervised Peptide Spectrum Match Rescoring

215 To assess the benefits of RT predictions, we used a semi-supervised support vector (SVM) machine  
216 model. The implementation is based on the python package scikit-learn<sup>58</sup> in which optimal  
217 parameters are determined via cross-validation. The input features were based on the initial search  
218 score (for FA-complex only) and differences between predicted and observed RTs. For each  
219 crosslinked peptide, three predictions were made per chromatographic dimension: for the  
220 crosslinked peptide, for the alpha peptide and the beta peptide. Additional features were engineered  
221 depending on the number of chromatographic dimensions and included the summed, absolute or

222 squared values of the initial features (Tab. S3 for all features). For example, for three RT dimensions,  
223 the total number of features was 43. The data for the training included all CSMs that passed the 1%  
224 CSM-FDR cutoff (self / heteromeric, TT, TD, DDs) and TD/DD identifications that did not pass this  
225 cutoff. TTs were labeled as positive training examples, TD and DDs (DXs) were labeled as negative  
226 training examples.

227 To stratify the  $k$ -folds during CV, the CSMs were binned into  $k$  xiSCORE percentiles. Afterwards, they  
228 were sampled such that each score range was equally represented across all CV folds. When the  
229 positive class was limited to the TT identifications at 1% CSM-FDR, the number of negative classes  
230 was usually larger than the number of positive classes. To circumvent this, for each CV split, a  
231 synthetic minority over-sampling technique (SMOTE)<sup>59</sup> was used to generate a balanced number of  
232 positive and negative training samples (here only used for the FA-complex data). SMOTE was applied  
233 within each CV fold to avoid information leakage. A 3-fold CV was performed for the rescoring. In  
234 each iteration during the CV, two folds were used for the training of the classifier and the third fold  
235 was used to compute an SVM score. During this CV step, a total of three classifiers were trained. The  
236 scores for all TT-CSMs that did not pass the initial FDR cutoff were computed by averaging the score  
237 predictions from the three predictors. For all CSMs passing the initial FDR cutoff, rescoring was  
238 performed when the CSM occurred in the test set during the CV. The final score was defined as:  
239  $x_{i_{rescored}} = x_{i_{SCORE}} + x_{i_{SCORE}} \times SVM_{score}$ , where  $SVM_{score}$  was the output from the SVM  
240 classifier and  $x_{i_{SCORE}}$  the initial search engine score.

## 241 Feature Analysis

242 The KernelExplainer from SHAP<sup>60</sup> (Shapley Additive exPlanations) was used to analyze the importance  
243 of features derived from the SVM classifier. SHAP estimates the importance of a feature by setting its  
244 value to “missing” for an observation in the testing set while monitoring the prediction outcome. We  
245 used a background distribution of 200 samples (100 TT, 100 TD) from the training data to simulate  
246 the “missing” status for a feature. SHAP values were then computed for 200 randomly selected TT  
247 (predicted to be TT) that were not used during the SVM training. SHAP values allow to directly

248 estimate the contributions of individual features towards a prediction, i.e. the expected value plus  
249 the SHAP values for a single CSM sums to the predicted outcome. For a selected CSM, a positive  
250 SHAP value contributes towards a true match prediction. For the interpretability analysis (SHAP) of  
251 the learned features in xiRT, the DeepExplainer was used (section S3).

252 In addition, we performed dimensionality reduction using UMAP<sup>61</sup> on the RT feature space for  
253 visualization purposes (excluding the search engine score). UMAP was run with default parameters  
254 ( $n\_neighbors=15$ ,  $min\_dist=0.1$ ) on the standardized feature values. The list of used features for the  
255 multi-task learning setup is available in Tab. S3.

## 256 Statistical Analysis

257 Significance tests were computed using a two-sided independent t-test with Bonferroni correction.  
258 The significance level  $\alpha$  was set to 5%.

## 259 Data Availability

260 The mass spectrometry proteomics data have been deposited to the ProteomeXchange Consortium  
261 (<http://proteomecentral.proteomexchange.org>) via the jPOST partner repository<sup>62‡</sup> with the dataset  
262 identifier PXD020407 and DOI 10.6019/PXD020407. Raw data of the FA-Complex is available via the  
263 previously published PRIDE identifier (PXD014282). Additional files and intermediate results are  
264 available via Zenodo (10.5281/zenodo.4270324). Source data are provided with this manuscript.

## 265 Code Availability

266 The developed python package is available on the python package index and on GitHub  
267 (<https://github.com/Rappsilber-Laboratory/xiRT>).

---

‡ Access: <https://repository.jpostdb.org/preview/1564483676042143f9d3ae>, key: 3194

## 268 Results and Discussion

269 This section covers 1) a description of the experimental workflow and the motivation, 2) the  
270 evaluation of the developed retention time predictor, 3) an interpretability analysis of the deep  
271 neural network, 4) an analysis of the RT features and their importance for rescoring, 5) the  
272 evaluation of the rescoring results from an *E. coli* lysate, and 6) the evaluation of the rescoring results  
273 from a routine crosslinking MS experiment, i.e. the analysis of a multiprotein complex (FA-complex).

### 274 A Substantial Fraction of Crosslinks below the Confidence Threshold are Correct

275 Crosslinked peptides belonging to the high-molecular weight *E. coli* proteome were deep-  
276 fractionated along three chromatographic dimensions (hSAX, SCX and RP). This 3D fractionation  
277 approach led to 144 LC-MS runs as some of the 90 fractions contained enough material for repeated  
278 analysis. The resulting data were searched with an entrapment database approach (Fig. 1a) leading  
279 to 11196 CSMs (11072 TT, 87 TD, 37 DD, Fig. S3) at 1% CSM-FDR, separating self and heteromeric  
280 CSMs<sup>16,44,63</sup>. The human entrapment database allows to assess error, independently of the target-  
281 decoy approach. This will play a critical role here as *E. coli* decoys will be used for the machine  
282 learning-based rescoring (but not for the RT prediction). Judged by a set of peptide characteristic  
283 metrics (e.g. peptide length, pI, GRAVY) the human entrapment database resembles the properties of  
284 the *E. coli* target database (Fig. S4).

285 Before attempting RT prediction and subsequent complementation of search scores, we investigated  
286 the extent of false negatives, approximated here by PPIs present in STRING<sup>47</sup> or APID<sup>46</sup> database. At  
287 1% CSM-FDR, 110 such ‘validated’ (val) protein-protein interactions were identified. 10%, 30% and  
288 50% CSM-FDR returned 226, 278 and 418 validated PPIs, respectively (Fig. 1b). When raising the  
289 CSM-FDR from 1% to 50% we thus saw a nearly 4-fold increase in the detectable number of validated  
290 PPIs. In contrast, using a pessimistic approach of semi-randomly drawing pairs of *E. coli* proteins from  
291 the STRING/APID (first protein) and the search database (second protein) yielded purely by chance  
292 10, 22, 44, and 91 overlapping PPIs with STRING or APID for 1%, 10%, 30% and 50% CSM-FDR cutoffs,



293 respectively. While this shows that loosening the FDR threshold increases validated PPIs also by  
294 chance, the actually observed number is much higher (418 versus 91 at 50% CSM-FDR). This means  
295 that there is a substantial number of valid PPIs with insufficient match confidence.

296 The underlying scoring challenge is essential to the identification of peptides in general. The plethora  
297 of search engines for linear<sup>64</sup> and crosslinked peptides<sup>65</sup> use spectral characteristics differently for  
298 their scoring. In xiSEARCH, the final score is a composite that incorporates spectral metrics such as  
299 explained intensity and matched number of fragments. Empirically, we observe a fast decrease in the  
300 search engine score (Fig. 1c) with increasing FDR. This indicates that at higher FDRs spectral matching  
301 metrics might be suboptimal. Poor spectral quality, inefficient peptide fragmentation or random  
302 fragment matching all influence the search engine score negatively. RT information could  
303 complement MS information but this would require accurate RT prediction of crosslinked peptides.

#### 304 **Accurate Multi-dimensional Retention Time Prediction for Crosslinked Peptides**

305 RT prediction for crosslinked peptides has not yet been achieved. One reason for this is the challenge  
306 of encoding a crosslinked pair of peptides for machine learning. We overcame this here using a  
307 Siamese neural network as part of a new machine learning application, xiRT (Fig. 1d), which allowed  
308 the incorporation of RTs into a rescoring workflow (Fig. 1e). The Siamese part of the network  
309 (embedding layer and recurrent layer) shares the same weights for both peptides. Practically, the  
310 sharing of weights leads to consistent predictions, independent of the peptide order. After the  
311 recurrent layer, the two outputs were combined and passed to three subnetworks consisting of  
312 dense layers with individual prediction layers (details on the architecture are available in Fig. S1). In  
313 this multi-task learning setup, the network simultaneously learned to predict the hSAX, SCX and RP  
314 RT through a single training step. Multi-task learning can improve the overall performance of  
315 predictors by forcing the network to learn a robust representation of the input data.<sup>66</sup>

316 The training and evaluation of xiRT followed a CV strategy that avoided the simultaneous learning  
317 and prediction on overlapping parts of the data (Methods, Fig. 2a). We used a 3-fold CV strategy

318 where two folds were used for training (excluding 10% for the validation throughout the training  
319 epochs) and one fold for testing/prediction. All CSMs with an FDR < 1% were used during CV. For the  
320 remaining CSMs, the best predictor (with the lowest total loss) was used to predict the RTs.

321 To achieve the best possible prediction performance, hyper-parameters of the network were  
322 optimized. Since extensive hyper-parameter optimization on a small data set can lead to overfitting,  
323 we initially optimized a large part of hyper-parameters using 20,802 unique linear peptide  
324 identifications at 1% FDR. The final parameters for the Siamese network architecture for crosslinks  
325 were obtained by a small grid-search (6,453 unique peptide-pairs at 1% CSM-FDR; Fig. S5).

326 Using these parameters, we evaluated the learning behavior during the training time (epochs) across  
327 the CV folds. The training behavior on the three CV folds was similar and reached a stable trajectory  
328 after approximately 15 epochs (Fig. 2b). Based on very similar error trends on validation and training  
329 sets, we concluded to have reached a state where neither overfitting nor underfitting occurred. The  
330 overall performance across the prediction folds was comparable in terms of accuracy (hSAX:  $61\% \pm$   
331  $1.1$ , SCX:  $47\% \pm 1.7$ ) and MSE ( $11.58 \pm 2.0$ )(Fig. 2c). Comparing single-task and multi-task  
332 configurations of xiRT revealed no significant differences in the prediction accuracy but greatly  
333 reduced run times (Fig. S6-7). Note that we estimated the theoretical boundaries given the  
334 ambiguous elution behavior (i.e. peptide elution across multiple chromatographic fractions) for SCX  
335 at 65% accuracy and for hSAX at 73% accuracy (Tab. S4, Fig. S8). Most of the predictions showed only  
336 a small error, and thus a high relaxed accuracy: for hSAX  $94\% \pm 0.0$  and for SCX  $87\% \pm 1.15$  of the  
337 predictions were within a range of  $\pm 1$  fraction (Fig. 2d-e). The  $R_{RP}^2$  of  $0.94 \pm 0.01$  also showed a  
338 predictable relationship for the RP dimension (Fig. 2f). The consistent accuracy and  $R^2$  results across  
339 CV folds demonstrates reproducible training and prediction behavior which reduces unwanted biases  
340 from the different CV folds. In conclusion, RTs of crosslinked peptides can robustly be learned within  
341 a data set, making them available as features in a CSM rescoring framework.

342 It was difficult to compare our RT predictions to other studies which used SCX<sup>67</sup> or hSAX<sup>29</sup> for multiple  
343 reasons: 1) there is currently no other model that predicts the RT of crosslinked peptides, 2) the  
344 recent SSRCalc<sup>67</sup> study (SCX) for linear peptides used a much larger data set of 34,454 unique  
345 peptides and the fractionation was much more fine-grained (30 - 50 fractions). Similarly, the hSAX<sup>29</sup>  
346 study on linear peptides used a much finer fractionation (30 fractions) and a different methodology  
347 to encode the loss function during the machine learning. 3) Applied gradients and liquid  
348 chromatography conditions can change the elution behavior quite drastically. In our study, the  
349 number of observations was neither for hSAX nor for SCX equally distributed but varied between  
350 ~200 and ~2000 CSMs per fraction (Fig. S3). Since we employed a partially exponential gradient  
351 during the chromatographic fractionation, the degree of peptide separation varied for earlier and  
352 later fractions.

353 Given that we had less data to train on than recent RT predictions of linear peptides, we evaluated  
354 how the numbers of observations influenced the prediction accuracy ( $R_{RP}^2 + Acc_{hsax} + Acc_{scx}$ , Fig.  
355 2g). The learning curve showed two important characteristics: first, the prediction performance over  
356 CV folds was very reproducible. This means that predictions were robust even with very moderate  
357 data quantity. Second, the maximal performance was achieved with approximately 70%-100% of the  
358 data points (100% corresponding to 6453 total CSMs, 3871 for training, 431 for validation, 2151 for  
359 prediction). Given that a first plateau was reached with 30% of the data, it is unclear if the final  
360 prediction accuracy constitutes another local optimum or the limit of the prediction accuracy. The  
361 individual task metrics showed that the RP behavior seemed to be easier for the model to learn than  
362 the ordinal regression tasks (SCX, hSAX, Fig. S9). The RP behavior could be accurately predicted from  
363 approximately 60% of the data points, while the maximum accuracy for hSAX and SCX dimensions  
364 was only achieved by using 80% - 100% of the data. In other words, while using even fewer CSMs  
365 might be possible when predicting RP RTs, one would expect a reduced accuracy in the hSAX/SCX  
366 dimensions.

367 An approach to reduce the number of required CSMs would be to leverage the abundantly available  
368 data on linear peptides for transfer learning. Indeed, a recent study showed that transfer learning  
369 across different peptide identification results works well for linear peptides<sup>34</sup>. However, in our hands,  
370 pretraining a network from linear peptides and applying the same weights to the Siamese part of the  
371 network neither improved the performance nor reduced the training time for crosslink RT predictions  
372 (data not shown). In contrast, a robust and accurate RT prediction could be achieved on a  
373 multiprotein complex crosslinking study (FA-complex, see below) when first training on the *E. coli*  
374 CSMs (Fig. S10). Another possibility to increase the training data size and robustness during CV is to  
375 increase the number of folds, e.g. 5- or 10-fold, at the cost of runtime. Increasing the expedience of  
376 xiRT, we also implemented transfer learning for cases when the number of fractions differs between  
377 the initial model and the new prediction task.

## 378 Explainable Deep Learning Reveals Amino Acid Contributions

379 Using the SHAP package, we set out to explain predictions made by xiRT. For instance, when a  
380 specific crosslinked peptide was analyzed, residue-specific contributions towards the predicted RT  
381 could be computed (Fig. S11). The residues D, E, Y and F displayed high SHAP values indicating a  
382 stronger retention during hSAX separation in a randomly chosen peptide. Looking at a specific  
383 crosslinked peptide in SCX (Fig. S12), the SHAP values highlighted that K and R were the most  
384 important residues contributing towards later peptide elution. As one might expect, crosslinked K  
385 residues contributed much less towards later elution times than the stronger charged, unmodified K  
386 residues. Investigating the SHAP values for a collection of CSMs revealed additional contributions  
387 from W for hSAX and H for SCX while returning hydrophobic residues Y, F, W, I, L, V and M for RP (Fig.  
388 S13), revealing residue contributions in crosslinked peptides as seen in the respective analyses of  
389 linear peptides<sup>29,67,68</sup>. In summary, the SHAP values were good estimates for the individual RT  
390 contributions of the amino acid residues.

391 Next, we investigated the network architecture and the learned feature representations more closely  
392 (Section S4). As first analysis, the dimensionality reduced embedding space across the network was

393 analyzed (Fig. S14). This revealed that the shared sequence-specific layer already captured the RP  
394 properties quite well, while the hSAX and SCX properties were not as clearly captured. As expected,  
395 the separation of CSMs according to RT increased the further the features propagated through the  
396 network. In the last layer, the RP and hSAX sub-networks reached a very good separation, while in  
397 the SCX subtask CSMs remained moderately separated in two dimensions.

## 398 RT Characteristics for Unsupervised Separation of True and False CSMs

399 Now that we established the RT prediction of crosslinked peptides, we computed a set of  
400 chromatographic features to explore their ability to separate true from false CSMs (Tab. S3).  
401 Dimensionality reduction was computed for RP only (13 chromatographic features) and for SCX-  
402 hSAX-RP (43 chromatographic features) predictions (Fig. 3a-b). Both chromatographic feature sets  
403 revealed good separation possibilities for confident TT (99% true, given 1% CSM-FDR) and TD (100%  
404 false) identifications in two-dimensional space. For the RP analysis, the TD *E. coli* CSMs and TT Mix /  
405 TD Mix CSMs were enriched in one area of the plot (the lower right part, Fig. 3a). In contrast, the  
406 subset of confident TT *E. coli* CSMs were distributed outside this area. As one would expect for two  
407 sets of random matches, the CSMs from the entrapment database (TT Mix, TD Mix) closely followed  
408 the distribution of TD *E. coli* CSMs. The areas populated by the known false matches were also  
409 populated by an equal number of presumably false TT matches. When the features of all three RT  
410 dimensions were considered, the separation of true and false CSMs further improved (Fig. 3b). Again,  
411 the distributions of TD *E. coli* CSMs and entrapment CSMs behaved similarly. Interestingly, few CSMs  
412 that passed the 1% FDR threshold were located in regions dominated by false identifications. This  
413 might identify them as part of the expectable fraction of 1% false positive identifications.  
414 Importantly, the described separation was achieved unsupervised on RT features alone, i.e. without a  
415 search engine score or target-decoy labels.

416 To test the transferability of our findings, we also ran xiRT with unfiltered pLink2 results (section S4  
417 and Fig. S15). The prediction performance from Q-value filtered CSMs was similar to the results with  
418 xiSEARCH (Fig. S15a-c). A two-sided t-test between hSAX, SCX and RP errors for TT and TDs revealed

419 significant differences in the respective error distributions of the pLink2 predictions (Fig. S15d).  
420 Importantly, the separation of true and false matches in two-dimensional space was also possible  
421 with pLink2 identifications (Fig. S15e). In summary, xiRT can learn retention times irrespective of the  
422 used search engine and the learned chromatographic features alone carry substantial information to  
423 separate true from false matches.

424 To investigate the relevance of multi-dimensional RT predictions for the identification of crosslinked  
425 peptides, we first supplemented each CSM with RT features. Then, we performed a semi-supervised  
426 rescoring and evaluated the trained SVM model using the SHAP framework. We chose to analyze  
427 SHAP values for the 15 most important features for TT observations (FDR > 1%) that were predicted  
428 to be a correct TT identification (Fig. 3c). This analysis revealed a similar magnitude for all 15 SHAP  
429 values implying that a single feature alone is insufficient to recognize false matches. Notably, the top  
430 5 features contained features from RP, hSAX and SCX predictions which indicates that each  
431 chromatographic dimension carried relevant information for the rescoring. Because 11 of the 15  
432 features were predictions considering only one of the two peptides and not directly derived from  
433 peptide-pairs, the predicted RTs displayed a larger error. This analysis suggests that an RT prediction  
434 model for linear peptides can add valuable information for crosslink analysis. In general, the model  
435 learned mostly that low errors in the RT dimensions indicate true positive identifications. Thus, the  
436 model implicitly learned that the RT of a crosslinked peptide should differ from the RT of the  
437 individual peptides. This might become useful especially for distinguishing consecutive<sup>45</sup> from  
438 crosslinked peptides or when dealing with gas-phase associated peptides<sup>36</sup>.

### 439 Rescoring Crosslinked Peptides Enhances their Identification

440 Before computing a combined score, we compared the CSM scores based on mass spectrometric  
441 information (xiSCORE) and RT features (SVM score, Fig. 4a). Both scores largely agreed. Heteromeric  
442 CSMs passing 1% CSM-FDR yielded high SVM scores. Also, most target-decoy CSMs achieved a low  
443 SVM score (Fig. 4a, right) and a low xiSCORE (Fig. 4a, top). The SVM score distribution of the TDs  
444 matched closely the distribution of TTs in the low scoring area, which indicated that they still

445 modeled random TT matches and that overfitting was avoided. Interestingly, the TTs were  
446 overrepresented in the low scoring area for the xiSCORE but not for the SVM score, suggesting that  
447 true TTs remained hidden among the random matches when using xiSCORE alone. The broad SVM  
448 score distribution of TTs indicated that the rescoring process could be optimized. In conclusion,  
449 neither of the mass spectrometric information (xiSCORE) nor the RT information (SVM score) seem to  
450 reveal all true CSMs.

451 As a combination of both approaches should yield better results than either alone, we combined the  
452 SVM score with the xiSCORE. We evaluated the impact of rescoring CSMs on the number and quality  
453 of identified PPIs, as PPIs are typically the objective of large-scale crosslinking MS experiments.  
454 Heteromeric CSMs increased by 1.7-fold and heteromeric PPIs increased by 1.4-fold (Fig. 4b). Self-  
455 links increased only marginally in agreement with their smaller search space and accordingly lower  
456 random match frequency. Essentially, nearly all self-links were identified exhaustively based on mass  
457 spectrometric data alone. In contrast, RT information substantially improved the identification of  
458 heteromeric CSMs. Further gains might be possible by directly combining RT features with mass  
459 spectrometric features (and possibly also other) for supervised scoring.

460 Likely, the benefits of RT predictions for the rescoring depend on the data set and applied  
461 chromatographic separations. On the *E. coli* data, we therefore performed additional analyses where  
462 we limited the rescoring to only use a subset of the chromatographic dimensions (Tab. S5). The  
463 number of identified CSMs for heteromeric links increased from 724 in the reference to 902 (RP  
464 only), 977 (SCX-RP), 1092 (hSAX-RP) and 1199 (SCX-hSAX-RP). Likewise, PPIs increased from 109 to  
465 135, 131, 157, 152, respectively (Tab. S5). As observed above, gains can be expected from each  
466 chromatographic dimension. When having to choose one ion chromatography, the hSAX dimension  
467 seemed more useful than the SCX dimension which could arise from the better prediction  
468 performance or more complex separation mechanisms. Importantly, even using RP RT alone already  
469 led to a marked gain in heteromeric PPIs (see also next section).

470 To systematically evaluate the additionally identified PPIs from all three RT dimensions, we  
471 compared them to the originally identified PPIs based exclusively on xiSCORE. In addition, the  
472 STRING/APID databases and a larger set of PPIs from a larger study<sup>16</sup> served as extra references for  
473 validation. Almost all PPIs found in the original dataset by xiSCORE were also contained in the  
474 rescored data set (91%). 85% of the newly identified PPIs were either found in the data set from Lenz  
475 *et al.*, in STRING/APID or both. Among the eight PPIs unique to the rescored data set, only one  
476 involved a human protein from the entrapment database (Fig. 4c). The remaining seven PPIs might  
477 constitute genuine PPIs. Note that the overall percentage of PPIs involving human proteins was  
478 reduced by rescoring. Since all human target proteins were included in the positive training data, this  
479 is an important indicator of a well-behaved model. Deepening trust further, almost all novel PPIs  
480 were identified with multiple CSMs (Fig. 4d). Finally, we selected the subnetwork of the RNA  
481 polymerase to investigate the additionally identified PPIs in a well-characterized interaction  
482 landscape (Fig. 4e). Indeed, all interactions added by RT-based rescoring were already reported in  
483 APID. In summary, all our evidence points at the successful complementation of MS information by  
484 RT, at least for a proteome-wide crosslinking analysis. It remained to be seen, however, if this could  
485 also be leveraged in more routine multiprotein complex analyses.

## 486 Multiprotein Complex Studies Also Benefit from the RT Prediction

487 Many crosslinking MS studies investigate multiprotein complexes and rely on only few  
488 chromatographic dimensions. We therefore evaluated the benefit of predicted RTs for the analysis of  
489 the FA-complex, an eight-membered multiprotein complex that was crosslinked using BS3. Here, the  
490 search engine score was supplemented exclusively with RP RT predictions during the rescoring. By  
491 using transfer learning, the small number of CSMs (692 unique CSMs, without considering charge  
492 states) found in this multiprotein complex analysis were sufficient to achieve accurate RP predictions  
493 (Fig. S10). The resulting crosslinks at 1% residue-pair FDR (lower levels set to 5%) showed an increase  
494 of 36 (+10%) self- and 53 (+70%) heteromeric residue-pairs. Importantly, the rescored links showed  
495 no indication of increased hits to the entrapment database (Fig. 5a) indicating that no overfitting



496 occurred during the rescoring. At the same time, heteromeric PPIs already identified before rescoring  
497 received additional support. For example, the number and sequence coverage of links increased  
498 between FAAP100 (“100”) and FANCB (“B”), FANCA (“A”) and FANCB, and FANCA and FANCG (“G”).  
499 Overall, the heteromeric links increased 1.7-fold with an even higher proportional increase in  
500 ‘verified’ links, i.e. fitting the available structure, by 1.9-fold (Fig. 5b). The derived distance  
501 distribution of newly identified links is dissimilar from a random distribution and shows no  
502 indications of reduced quality (Fig. 5c). Applying this ‘structural validation’ on its own might be  
503 optimistic<sup>69</sup>, however, in summary our rigorous quality control ensures trustworthy results. It is  
504 currently unclear in how far even smaller datasets could benefit from xiRT. Generally, to improve  
505 prediction performance, pre-training on larger data sets will lead to better generalization abilities of  
506 the predictor. Subsequently, also smaller data sets can be used for accurate RT prediction. To  
507 additionally benefit from sample specific information, increasing the cross-validation splits will utilize  
508 larger parts of the data during training. In any case, our successful analysis of a multiprotein complex  
509 supplemented with only RP features highlights the broad applicability of xiRT.

## 510 Conclusion

511 Using a Siamese network architecture, we succeeded in bringing RT prediction into the Crosslinking  
512 MS field, independent of separation setup and search software. Our open source application xiRT  
513 introduces the concept of multi-task learning to achieve multi-dimensional chromatographic  
514 retention time prediction, and may use any peptide sequence-dependent measure including for  
515 example collision cross section or isoelectric point. The black-box character of the neural network  
516 was reduced by means of interpretable machine learning that revealed individual amino acid  
517 contributions towards the separation behavior. The RT predictions – even when using only the RP  
518 dimension – complement mass spectrometric information to enhance the identification of  
519 heteromeric crosslinks in multiprotein complex and proteome-wide studies. Overfitting does not  
520 account for this gain as known false target matches from an entrapment database did not increase.

521 Leveraging additional information sources may help to address the mass-spectrometric identification  
522 challenge of heteromeric crosslinks.

## 523 Acknowledgements

524 We thank Edward Rullmann, Andrea Graziadei and Francis O'Reilly for critical reading of the  
525 manuscript, and Jakub Bartoszewicz (RKI / HPI) for fruitful discussions. We are grateful to Tabea  
526 Schütze for help with fermenting *E. coli*.

## 527 Funding Sources

528 This work was supported by NVIDIA with hardware from the grant "Artificial Intelligence for Deep  
529 Structural Proteomics", by the Wellcome Trust through a Senior Research Fellowship to JR (103139)  
530 and by the Deutsche Forschungsgemeinschaft (DFG, German Research Foundation) under Germany's  
531 Excellence Strategy - EXC 2008 - 390540038 – UniSysCat, and by grant no. 392923329/GRK2473. The  
532 Wellcome Centre for Cell Biology is supported by core funding from the Wellcome Trust (203149).

## 533 Additional Information

### 534 Abbreviations

535 FDR, false discovery rate; RT, Retention time; hSAX, hydrophilic strong anion exchange  
536 chromatography; SCX, strong cation exchange chromatography; RP, Reversed-phase chromatography;  
537 CV, cross-validation; acc, accuracy; racc, relaxed accuracy; TT, target-target; TD, target-decoy; DD,  
538 decoy-decoy; PPI, protein-protein interaction.

### 539 Supplementary Information

540 Identifications over the different gradients, details on the network architecture/the hyper-parameter  
541 optimization, machine learning results for linear peptide identifications, learning curves, RT error

542 characteristics, xiRT explainability analysis, results from combining pLink2 and xiRT are available in  
543 the supplementary material.

## 544 Corresponding Author

545 \*Juri Rappsilber: [juri.rappsilber@tu-berlin.de](mailto:juri.rappsilber@tu-berlin.de)

## 546 References

- 547 1. O'Reilly, F. J. & Rappsilber, J. Cross-linking mass spectrometry: methods and applications in  
548 structural, molecular and systems biology. *Nat. Struct. Mol. Biol.* **25**, 1 (2018).
- 549 2. Yu, C. & Huang, L. Cross-Linking Mass Spectrometry: An Emerging Technology for  
550 Interactomics and Structural Biology. *Anal. Chem.* **90**, 144–165 (2018).
- 551 3. Leitner, A., Faini, M., Stengel, F. & Aebersold, R. Crosslinking and Mass Spectrometry: An  
552 Integrated Technology to Understand the Structure and Function of Molecular Machines.  
553 *Trends in Biochemical Sciences* (2016) doi:10.1016/j.tibs.2015.10.008.
- 554 4. Trnka, M. J., Baker, P. R., Robinson, P. J. J., Burlingame, a L. & Chalkley, R. J. Matching Cross-  
555 linked Peptide Spectra: Only as Good as the Worse Identification. *Mol. Cell. Proteomics* **13**,  
556 420–434 (2014).
- 557 5. Giese, S. H., Fischer, L. & Rappsilber, J. A Study into the Collision-induced Dissociation (CID)  
558 Behavior of Cross-Linked Peptides. *Mol. Cell. Proteomics* **15**, 1094–1104 (2016).
- 559 6. Barysz, H. M. & Malmström, J. Development of Large-scale Cross-linking Mass Spectrometry.  
560 *Molecular and Cellular Proteomics* (2018) doi:10.1074/mcp.R116.061663.
- 561 7. Rinner, O. *et al.* Identification of cross-linked peptides from large sequence databases. *Nat.*  
562 *Methods* **5**, 315–8 (2008).
- 563 8. Chen, Z. A. *et al.* Architecture of the RNA polymerase II-TFIIF complex revealed by cross-  
564 linking and mass spectrometry. *EMBO J.* **29**, 717–26 (2010).
- 565 9. Liu, F., Rijkers, D. T. S., Post, H. & Heck, A. J. R. Proteome-wide profiling of protein assemblies  
566 by cross-linking mass spectrometry. *Nat. Methods* **12**, 1179–1184 (2015).
- 567 10. Schweppe, D. K. *et al.* Mitochondrial protein interactome elucidated by chemical cross-linking  
568 mass spectrometry. *Proc. Natl. Acad. Sci.* **114**, 1732–1737 (2017).
- 569 11. Leitner, A., Walzthoeni, T. & Aebersold, R. Lysine-specific chemical cross-linking of protein  
570 complexes and identification of cross-linking sites using LC-MS/MS and the xQuest/xProphet  
571 software pipeline. *Nat. Protoc.* **9**, 120–137 (2014).
- 572 12. Mendes, M. L. *et al.* An integrated workflow for crosslinking mass spectrometry. *Mol. Syst.*  
573 *Biol.* **15**, e8994 (2019).
- 574 13. Götze, M., Iacobucci, C., Ihling, C. H. & Sinz, A. A Simple Cross-Linking/Mass Spectrometry  
575 Workflow for Studying System-wide Protein Interactions. *Anal. Chem.* **91**, 10236–10244  
576 (2019).
- 577 14. Ryl, P. S. J. *et al.* In Situ Structural Restraints from Cross-Linking Mass Spectrometry in Human  
578 Mitochondria. *J. Proteome Res.* **19**, 327–336 (2020).

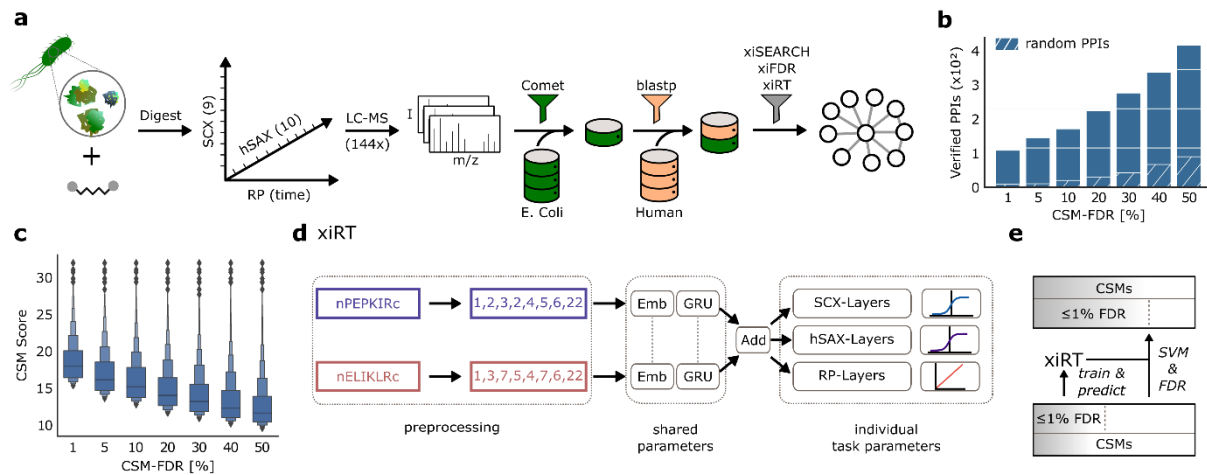
- 579 15. O'Reilly, F. J. *et al.* In-cell architecture of an actively transcribing-translating expressome.  
580 *Science* (80-. ). **369**, 554–557 (2020).
- 581 16. Lenz, S. *et al.* Reliable identification of protein-protein interactions by crosslinking mass  
582 spectrometry. *BioRxiv* 1–10 (2020) doi:10.1101/2020.05.25.114256.
- 583 17. Gonzalez-Lozano, M. A. *et al.* Stitching the synapse: Cross-linking mass spectrometry into  
584 resolving synaptic protein interactions. *Sci. Adv.* **6**, eaax5783 (2020).
- 585 18. The, M., MacCoss, M. J., Noble, W. S. & Käll, L. Fast and Accurate Protein False Discovery  
586 Rates on Large-Scale Proteomics Data Sets with Percolator 3.0. *J. Am. Soc. Mass Spectrom.* **27**,  
587 1719–1727 (2016).
- 588 19. Granholm, V., Noble, W. S. & Käll, L. A cross-validation scheme for machine learning  
589 algorithms in shotgun proteomics. *BMC Bioinformatics* **13 Suppl 1**, S3 (2012).
- 590 20. Hoopmann, M. R. *et al.* Kojak: efficient analysis of chemically cross-linked protein complexes.  
591 *J. Proteome Res.* **14**, 2190–8 (2015).
- 592 21. Keller, A., Nesvizhskii, A. I., Kolker, E. & Aebersold, R. Empirical Statistical Model To Estimate  
593 the Accuracy of Peptide Identifications Made by MS/MS and Database Search. *Anal. Chem.* **74**,  
594 5383–5392 (2002).
- 595 22. Ma, K., Vitek, O. & Nesvizhskii, A. I. A statistical model-building perspective to identification of  
596 MS/MS spectra with PeptideProphet. *BMC Bioinformatics* **13**, S1 (2012).
- 597 23. Liu, F., Lössl, P., Scheltema, R., Viner, R. & Heck, A. J. R. Optimized fragmentation schemes and  
598 data analysis strategies for proteome-wide cross-link identification. *Nat. Commun.* (2017)  
599 doi:10.1038/ncomms15473.
- 600 24. Chen, Z.-L. *et al.* A high-speed search engine pLink 2 with systematic evaluation for proteome-  
601 scale identification of cross-linked peptides. *Nat. Commun.* **10**, 3404 (2019).
- 602 25. Klammer, A. A., Yi, X., MacCoss, M. J. & Noble, W. S. Improving tandem mass spectrum  
603 identification using peptide retention time prediction across diverse chromatography  
604 conditions. *Anal. Chem.* **79**, 6111–8 (2007).
- 605 26. Dwivedi, R. C. *et al.* Practical implementation of 2D HPLC scheme with accurate peptide  
606 retention prediction in both dimensions for high-throughput bottom-up proteomics. *Anal.*  
607 *Chem.* **80**, 7036–42 (2008).
- 608 27. Krokhin, O. V. Sequence-Specific Retention Calculator. Algorithm for Peptide Retention  
609 Prediction in Ion-Pair RP-HPLC: Application to 300- and 100-Å Pore Size C18 Sorbents. *Anal.*  
610 *Chem.* **78**, 7785–7795 (2006).
- 611 28. Pfeifer, N., Leinenbach, A., Huber, C. G. & Kohlbacher, O. Improving peptide identification in  
612 proteome analysis by a two-dimensional retention time filtering approach. *J. Proteome Res.* **8**,  
613 4109–15 (2009).
- 614 29. Giese, S. H., Ishihama, Y. & Rappsilber, J. Peptide Retention in Hydrophilic Strong Anion  
615 Exchange Chromatography Is Driven by Charged and Aromatic Residues. *Anal. Chem.*  
616 [acs.analchem.7b05157](https://doi.org/10.1021/acs.analchem.7b05157) (2018) doi:10.1021/acs.analchem.7b05157.
- 617 30. Alpert, A. J. *et al.* Peptide orientation affects selectivity in ion-exchange chromatography.  
618 *Anal. Chem.* **82**, 5253–9 (2010).
- 619 31. Yeung, D., Klaassen, N., Mizero, B., Spicer, V. & Krokhin, O. V. Peptide retention time  
620 prediction in hydrophilic interaction liquid chromatography: Zwitter-ionic sulfoalkylbetaine  
621 and phosphorylcholine stationary phases. *J. Chromatogr. A* (2020)

- 622 doi:10.1016/j.chroma.2020.460909.
- 623 32. Ba, L. J. & Caruana, R. Do Deep Nets Really Need to be Deep? *Nature* **521**, 436–444 (2013).
- 624 33. Tran, N. H., Zhang, X., Xin, L., Shan, B. & Li, M. De novo peptide sequencing by deep learning.  
625 *Proc. Natl. Acad. Sci. U. S. A.* (2017) doi:10.1073/pnas.1705691114.
- 626 34. Ma, C. *et al.* Improved Peptide Retention Time Prediction in Liquid Chromatography through  
627 Deep Learning. *Anal. Chem.* **90**, 10881–10888 (2018).
- 628 35. Gessulat, S. *et al.* ProSIT: proteome-wide prediction of peptide tandem mass spectra by deep  
629 learning. *Nat. Methods* **16**, 509–518 (2019).
- 630 36. Giese, S. H., Belsom, A., Sinn, L., Fischer, L. & Rappsilber, J. Noncovalently Associated Peptides  
631 Observed during Liquid Chromatography-Mass Spectrometry and Their Affect on Cross-Link  
632 Analyses. *Anal. Chem.* **91**, 2678–2685 (2019).
- 633 37. Giese, S. H., Belsom, A. & Rappsilber, J. Optimized fragmentation regime for diazirine photo-  
634 cross-linked peptides. *Anal. Chem.* **88**, 8239–8247 (2016).
- 635 38. Liu, F., Lössl, P., Scheltema, R., Viner, R. & Heck, A. J. R. Optimized fragmentation schemes and  
636 data analysis strategies for proteome-wide cross-link identification. *Nat. Commun.* **8**, 15473  
637 (2017).
- 638 39. Rappsilber, J., Ishihama, Y. & Mann, M. Stop and go extraction tips for matrix-assisted laser  
639 desorption/ionization, nanoelectrospray, and LC/MS sample pretreatment in proteomics.  
640 *Anal. Chem.* **75**, 663–70 (2003).
- 641 40. Kessner, D., Chambers, M., Burke, R., Agus, D. & Mallick, P. ProteoWizard: open source  
642 software for rapid proteomics tools development. *Bioinformatics* **24**, 2534–6 (2008).
- 643 41. Eng, J. K. *et al.* A Deeper Look into Comet - Implementation and Features. *J. Am. Soc. Mass  
644 Spectrom.* (2015) doi:10.1007/s13361-015-1179-x.
- 645 42. Lenz, S., Giese, S. H., Fischer, L. & Rappsilber, J. In-Search Assignment of Monoisotopic Peaks  
646 Improves the Identification of Cross-Linked Peptides. *J. Proteome Res.* **17**, 3923–3931 (2018).
- 647 43. Koster, J. & Rahmann, S. Snakemake--a scalable bioinformatics workflow engine.  
648 *Bioinformatics* **28**, 2520–2522 (2012).
- 649 44. Fischer, L. & Rappsilber, J. Quirks of Error Estimation in Cross-Linking/Mass Spectrometry.  
650 *Anal. Chem.* **89**, 3829–3833 (2017).
- 651 45. Iacobucci, C. & Sinz, A. To Be or Not to Be? Five Guidelines to Avoid Misassignments in Cross-  
652 Linking/Mass Spectrometry. *Anal. Chem.* **89**, 7832–7835 (2017).
- 653 46. Alonso-López, Di. *et al.* APID database: Redefining protein-protein interaction experimental  
654 evidences and binary interactomes. *Database* **2019**, 1–8 (2019).
- 655 47. Szklarczyk, D. *et al.* STRING v11: Protein-protein association networks with increased  
656 coverage, supporting functional discovery in genome-wide experimental datasets. *Nucleic  
657 Acids Res.* (2019) doi:10.1093/nar/gky1131.
- 658 48. Storey, J. D. & Tibshirani, R. Statistical significance for genomewide studies. *Proc. Natl. Acad.  
659 Sci. U. S. A.* (2003) doi:10.1073/pnas.1530509100.
- 660 49. Altschul, S. F., Gish, W., Miller, W., Myers, E. W. & Lipman, D. J. Basic local alignment search  
661 tool. *J. Mol. Biol.* (1990) doi:10.1016/S0022-2836(05)80360-2.
- 662 50. Shakeel, S. *et al.* Structure of the Fanconi anaemia monoubiquitin ligase complex. *Nature* **575**,

- 663 234–237 (2019).
- 664 51. Farrell, D. P. *et al.* Deep learning enables the atomic structure determination of the Fanconi  
665 Anemia core complex from cryoEM. *IUCr* **7**, 881–892 (2020).
- 666 52. farrell, daniel. Deep learning enables the atomic structure determination of the Fanconi  
667 Anemia core complex from cryoEM. (2020) doi:10.5281/ZENODO.3998806.
- 668 53. Graham, M. J., Combe, C., Kolbowski, L. & Rappsilber, J. xiView: A common platform for the  
669 downstream analysis of Crosslinking Mass Spectrometry data. *bioRxiv* (2019)  
670 doi:10.1101/561829.
- 671 54. Pedregosa, F. *et al.* Scikit-learn: Machine Learning in Python. *J. Mach. Learn. Res.* **12**, 2825–  
672 2830 (2011).
- 673 55. Abadi, M. *et al.* TensorFlow: A system for large-scale machine learning. in *Proceedings of the*  
674 *12th USENIX Symposium on Operating Systems Design and Implementation, OSDI 2016* (2016).
- 675 56. Cheng, J., Wang, Z. & Pollastri, G. A neural network approach to ordinal regression. in  
676 *Proceedings of the International Joint Conference on Neural Networks* (2008).  
677 doi:10.1109/IJCNN.2008.4633963.
- 678 57. Berrar, D. Cross-validation. in *Encyclopedia of Bioinformatics and Computational Biology: ABC*  
679 *of Bioinformatics* (2018). doi:10.1016/B978-0-12-809633-8.20349-X.
- 680 58. Pedregosa, F. *et al.* Scikit-learn: Machine Learning in Python. *J. Mach. Learn. Res.* **12**, 2825–  
681 2830 (2011).
- 682 59. Chawla, N. V., Bowyer, K. W., Hall, L. O. & Kegelmeyer, W. P. SMOTE: Synthetic minority over-  
683 sampling technique. *J. Artif. Intell. Res.* (2002) doi:10.1613/jair.953.
- 684 60. Lundberg, S. & Lee, S.-I. A Unified Approach to Interpreting Model Predictions. *Nips* **16**, 426–  
685 430 (2017).
- 686 61. McInnes, L., Healy, J., Saul, N. & Großberger, L. UMAP: Uniform Manifold Approximation and  
687 Projection. *J. Open Source Softw.* **3**, 861 (2018).
- 688 62. Okuda, S. *et al.* JPOSTrepo: An international standard data repository for proteomes. *Nucleic*  
689 *Acids Res.* (2017) doi:10.1093/nar/gkw1080.
- 690 63. Walzthoeni, T. *et al.* False discovery rate estimation for cross-linked peptides identified by  
691 mass spectrometry. *Nat. Methods* **9**, 901–903 (2012).
- 692 64. Xu, C. & Ma, B. Software for computational peptide identification from MS-MS data. *Drug*  
693 *Discovery Today* (2006) doi:10.1016/j.drudis.2006.05.011.
- 694 65. Yilmaz, Ş. *et al.* Cross-linked peptide identification: A computational forest of algorithms.  
695 *Mass Spectrom. Rev.* **37**, 738–749 (2018).
- 696 66. Ruder, S. An Overview of Multi-Task Learning in Deep Neural Networks. *arXiv* 1706.05098  
697 (2017).
- 698 67. Gussakovsky, D., Neustaeter, H., Spicer, V. & Krokhin, O. V. Sequence-Specific Model for  
699 Peptide Retention Time Prediction in Strong Cation Exchange Chromatography. *Anal. Chem.*  
700 **89**, 11795–11802 (2017).
- 701 68. Guo, D., Mant, C. T., Taneja, A. K., Parker, J. M. R. & Rodges, R. S. Prediction of peptide  
702 retention times in reversed-phase high-performance liquid chromatography I. Determination  
703 of retention coefficients of amino acid residues of model synthetic peptides. *J. Chromatogr. A*  
704 (1986) doi:10.1016/0021-9673(86)80102-9.

- 705 69. Yugandhar, K., Wang, T. Y., Wierbowski, S. D., Shayhidin, E. E. & Yu, H. Structure-based  
706 validation can drastically underestimate error rate in proteome-wide cross-linking mass  
707 spectrometry studies. *Nat. Methods* (2020) doi:10.1038/s41592-020-0959-9.  
708





709

710 **Figure 1: Workflow overview.** a) Experimental and data analysis workflow. The soluble high-

711 molecular weight proteome of *E. coli* lysate was crosslinked with disuccinimidyl suberate (DSS) and

712 the digest sequentially fractionated by SCX (9 fractions collected), hSAX (10 pools collected) and

713 finally by RP coupled to the MS. The protein database for the crosslink search was created by a linear

714 peptide search with Comet and a sequence-based filter using BLAST. For each *E. coli* protein in the

715 final database a human protein was added as a control. b) Potential for false negative PPI

716 identifications. Verified PPIs are estimated from matches to the STRING/APIID databases. PPIs are

717 computed based on CSM-level FDR. Estimated random hits correspond to the average number of

718 semi-randomly drawn pairs (first protein was randomly selected from the STRING/APIID DB and

719 second protein was drawn from the FASTA file). Gained PPIs accentuate the additional information

720 that is available in the data at higher FDR. c) Decrease of CSM scores based on spectral evidence with

721 increased FDRs. Boxenplot shows the median and 50% of the data in the central box. d) xiIRT network

722 architecture to predict multi-dimensional retention times. A crosslinked peptide is represented as

723 two individual inputs to xiIRT. xiIRT uses a Siamese network architecture that shares the weights of the

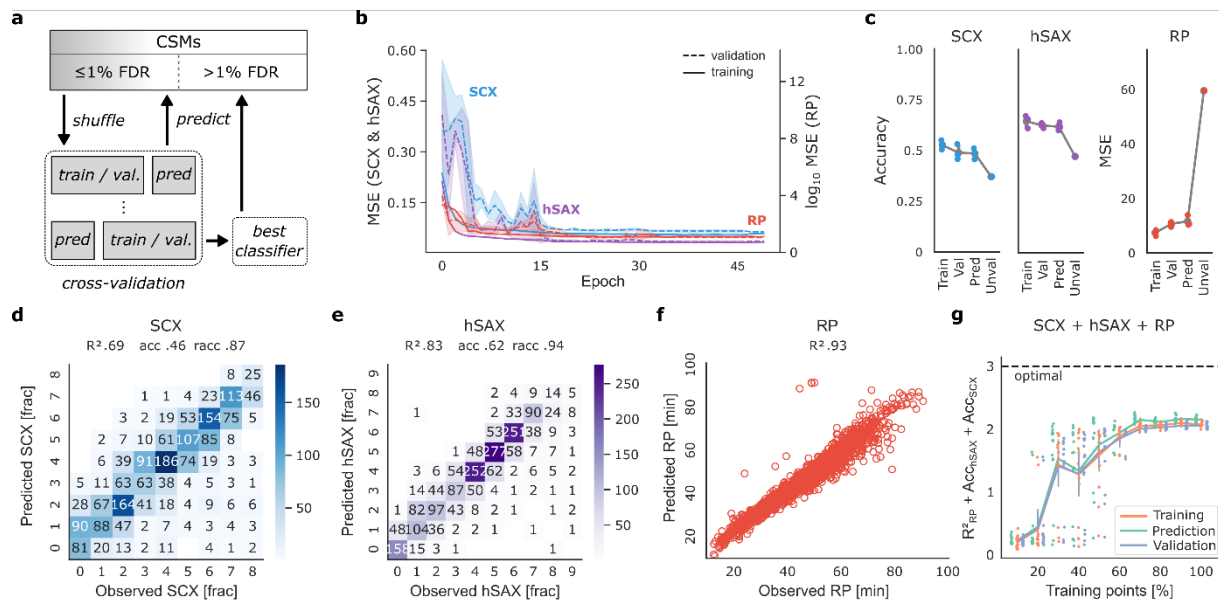
724 embedding and recurrent layers. Individual layers for the prediction tasks are added with custom

725 activation functions (sigmoid / linear functions for fractionation / regression tasks, respectively). e)

726 Rescoring workflow. The predictions from xiIRT are combined with xiSCORE's output to rescore CSMs

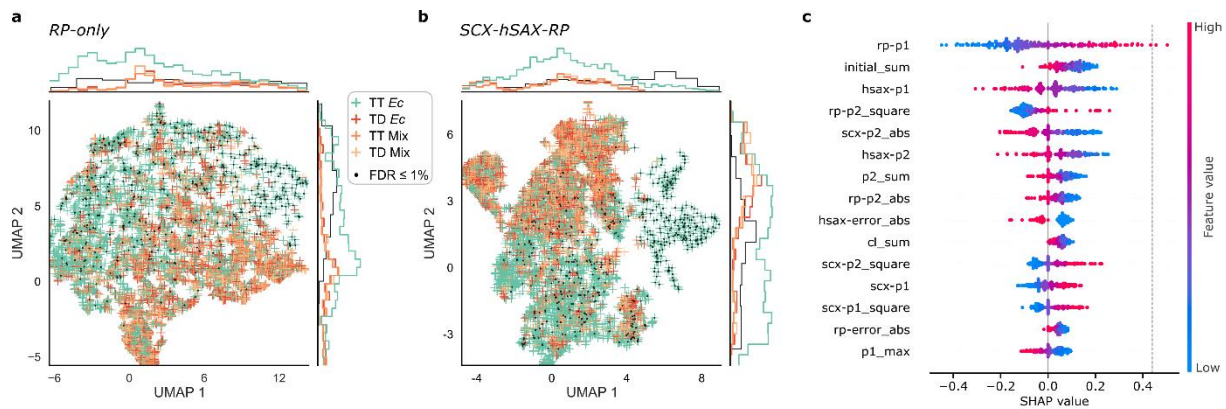
727 using a linear SVM, consequently leading to more matches at constant confidence.





728

729 **Figure 2: Cross-validation of retention time prediction.** a) Applied cross-validation strategy in xiRT. To  
 730 predict the RTs of CSMs excluded from training, the best CV classifier is used. b) xiRT performance  
 731 over training epochs. Shaded areas show the estimated 95% confidence interval. c) xiRT performance  
 732 across different metrics (error bars show standard deviation). Prediction for the ‘unvalidated’ data  
 733 was only performed once. d-f) Prediction results from a representative CV iteration for SCX, hSAX and  
 734 RP at 1% CSM-FDR. g) Learning curve with increasing number of CSMs, e.g. 10% (645 total CSMs, 387  
 735 for training, 43 for validation, 215 for prediction), 50% (3226, 1935, 216, 1075), 100% (6453, 3871,  
 736 431, 2151); bars indicate standard deviation.



737

738 **Figure 3: Visualization of RT features.** a) xiRT-based features from RP dimension only (13 features)

739 after dimensionality reduction with UMAP. b) xiRT-based feature from SCX-hSAX-RP dimensions (43

740 features) after dimensionality reduction with UMAP. Input data for a) and b) were CSMs of

741 heteromeric links in the proteome-wide crosslinking dataset (Ec = E. coli, Mix = match between E.

742 Coli and human peptides), filtered to 50% CSM-FDR. Identifications passing 1% CSM-FDR are

743 highlighted. DD identifications are not shown. c) SHAP analysis of RT feature importance for CSM-

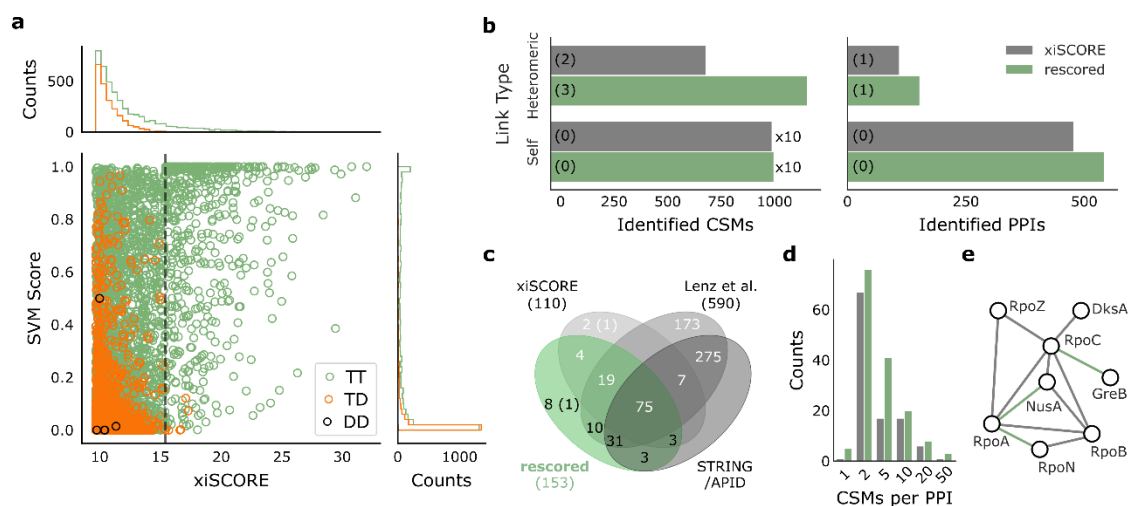
744 rescoring (using a linear SVM) including SCX, hSAX and RP features (Tab. S4). Each dot represents a

745 previously identified CSM from 200 randomly chosen TTs that were excluded from training (i.e. CSM-

746 FDR > 1%). The background data set consists of 100 TT and TD CSMs each. Dashed line indicates the

747 base value for a prediction based on the background data alone (0.44).

748



749

750 **Figure 4: Incorporation of RT prediction to CSM-scoring increases crosslink identification.** a) Score

751 distributions of heteromeric CSMs based on mass spectrometric information (xiSCORE) and RT

752 features (SVM score). The dashed line indicates the xiSCORE-based CSM-FDR threshold of 1%. b)

753 Increase in identification of TT-CSMs and PPIs at constant FDR. Numbers in brackets indicate

754 identifications involving a human protein. c) Overlap of observed PPIs (at 1% heteromeric PPI-FDR) to

755 external references. Numbers in the Venn diagram represent the identified PPIs among *E. coli*

756 proteins or PPIs involving human proteins (in brackets). Black numbers highlight the added benefit

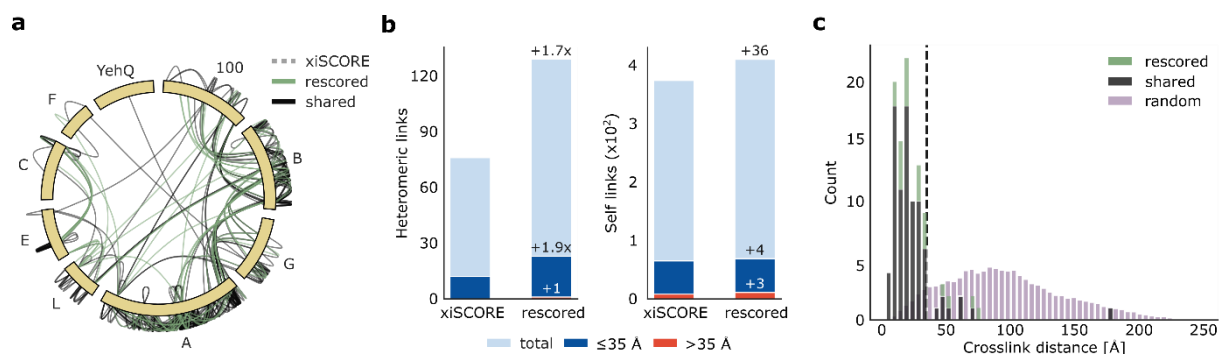
757 from combining xiSCORE with xiRT's SVM score for PPI identification. d) Distribution of CSMs per PPI

758 before (grey) and after CSM-rescoring (green). e) Selected subnetwork of the RNA polymerase with

759 PPIs only identified after the rescoring connected in green. Data in b-e corresponds to a 1% PPI-FDR

760 (prefiltered at a 5% CSM-FDR).

761



762

763 **Figure 5: Benefit of RT prediction for multiprotein complex crosslink analysis.** a) Crosslink network

764 from the Fanconi anemia complex analysis, shown in circular view. Unique residue pairs from

765 xiSCORE, after rescoring and shared between these analyses are depicted (1% residue-pair FDR).

766 Proteins associated to the Fanconi anemia core complex are indicated with their gene name suffix.

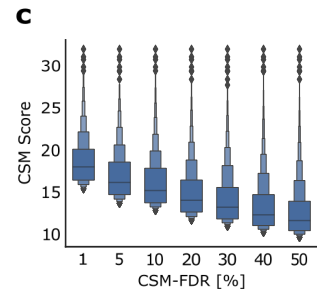
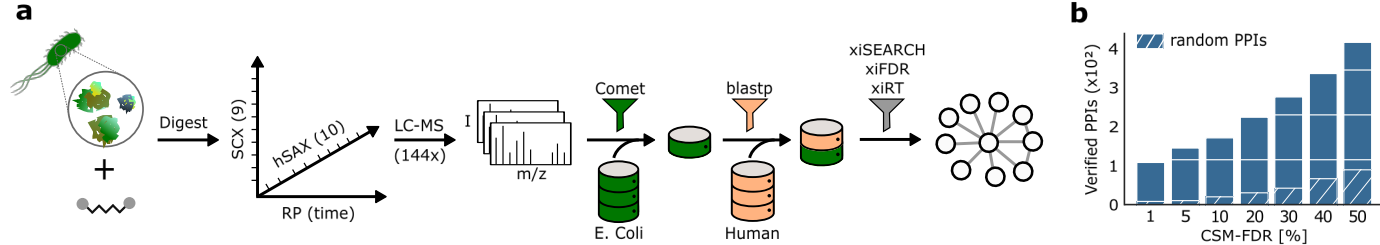
767 The *E. coli* protein YehQ represents a match from the entrapment database. b) Quantitative

768 assessment of residue-pairs with and without rescoring, and including calculated distances in the

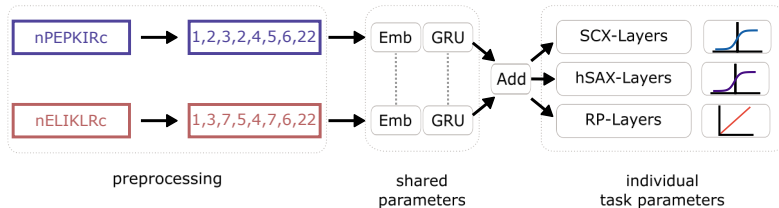
769 model. c) Distribution of crosslink distances from identified residue-pairs (n=105) following rescoring,

770 shared between rescoring and xiSCORE (since no crosslinks unique to xiSCORE), and theoretically

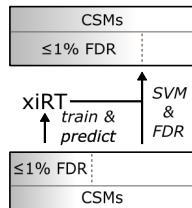
771 possible residue-pairs that could be mapped to the model.

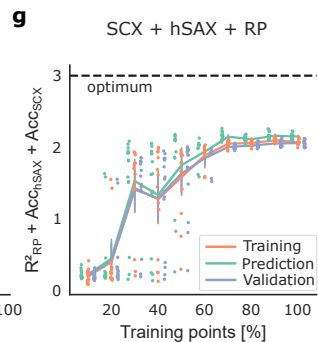
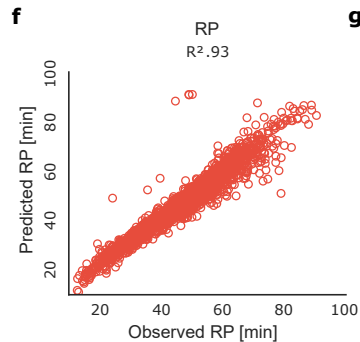
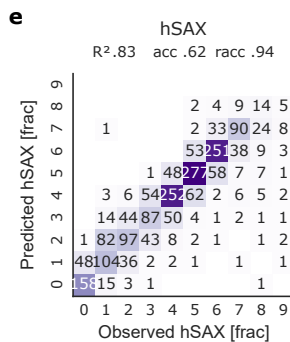
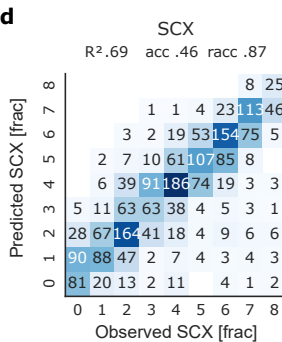
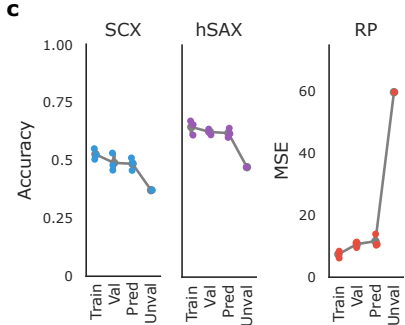
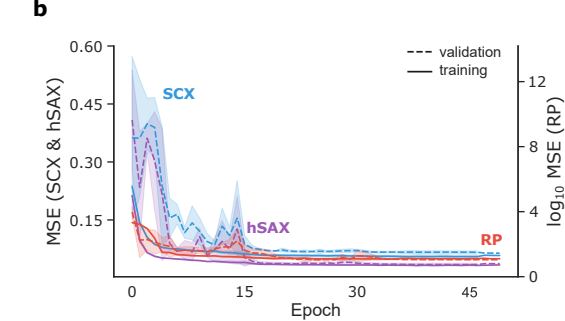
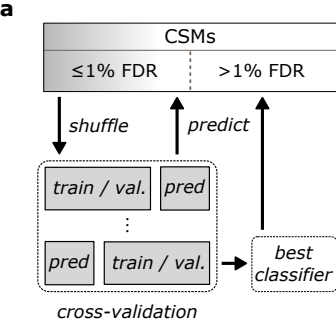


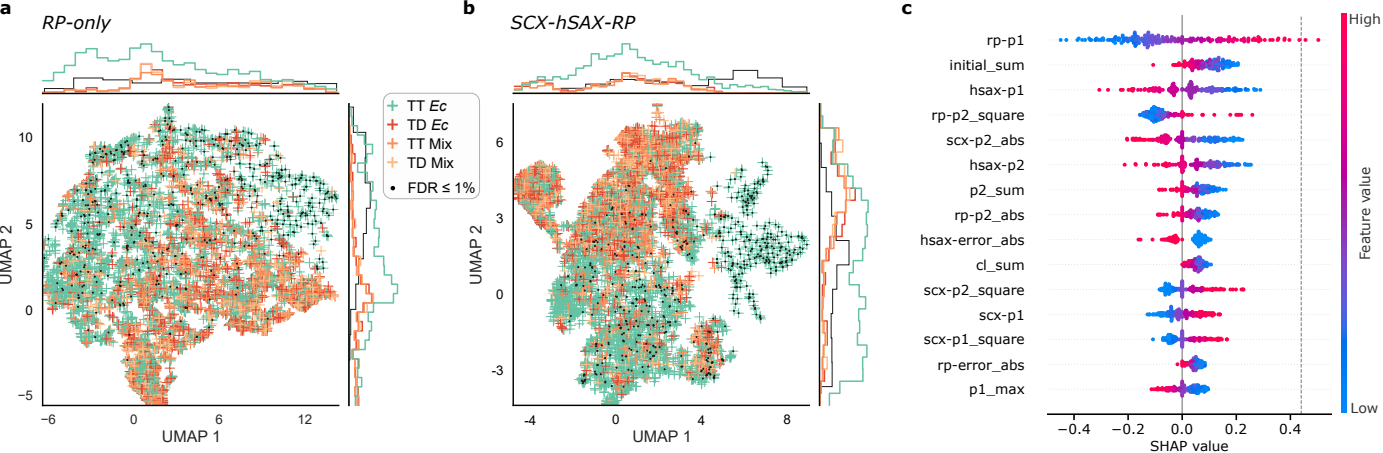
**d** xiRT

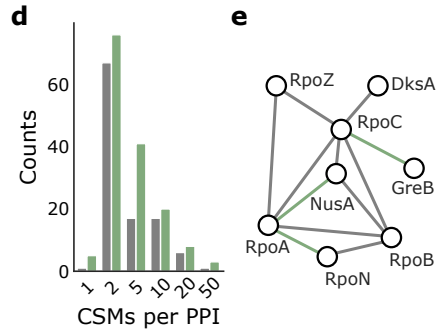
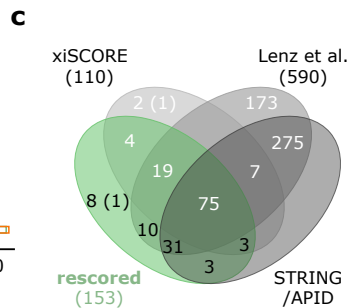
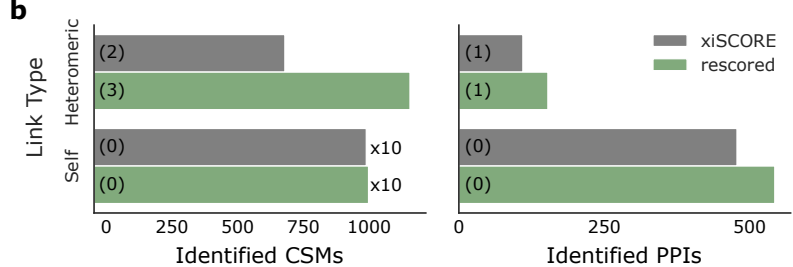
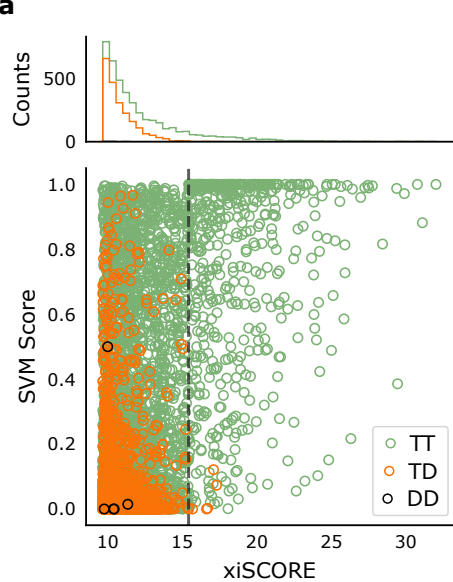


**e**

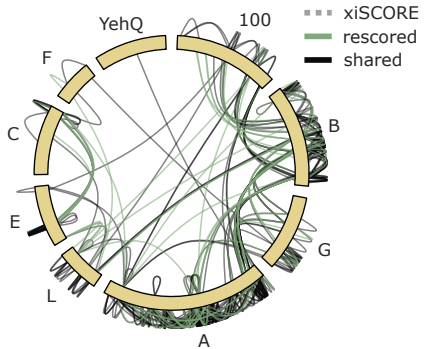
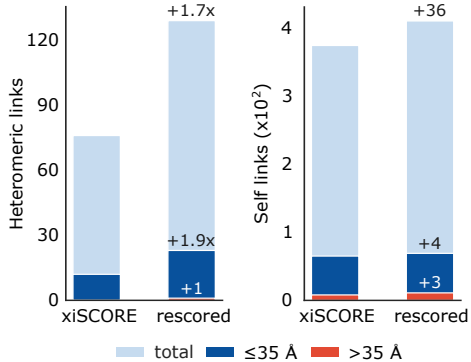










**a****b****c**